Inorganic Chemistry

Article

pubs.acs.org/IC

Two New Noncentrosymmetric (NCS) Polar Oxides: Syntheses, Characterization, and Structure–Property Relationships in $BaMTe_2O_7$ ($M = Mg^{2+}$ or Zn^{2+})

Jeongho Yeon, Sang-Hwan Kim, Sau Doan Nguyen, Hana Lee, and P. Shiv Halasyamani*

Department of Chemistry, University of Houston, 136 Fleming Building, Houston, Texas 77204-500, United States

Supporting Information

ABSTRACT: Two new noncentrosymmetric (NCS) polar oxides, $BaMgTe_2O_7$ and $BaZnTe_2O_7$, have been synthesized and characterized, with their crystal structures determined by single crystal X-ray diffraction. The iso-structural materials exhibit structures consisting of layers of corner-shared MgO_5 or ZnO_5, $Te^{6+}O_6$, and $Te^{4+}O_4$ polyhedra that are separated by Ba^{2+} cations. The Te^{4+} cation is found in a highly asymmetric and polar coordination environment attributable to its stereoactive lone-pair. The alignment of the individual TeO_4 polar polyhedra results in macroscopic polarity for $BaMgTe_2O_7$ and $BaZnTe_2O_7$. Powder second-harmonic generation (SHG) measurements revealed a moderate SHG efficiency of approximately 5 × KDP (or 200 × α-SiO_2) for both materials. Piezoelectric charge constants of 70 and 57 pm/V, and pyroelectric coefficients of −18 and −10 $\mu C \cdot m^{-2} \cdot K^{-1}$ were obtained for $BaMgTe_2O_7$ and $BaZnTe_2O_7$, respectively. Although the materials are polar, frequency dependent polarization measurements indicated that the materials are *not* ferroelectric, that is, the observed macroscopic polarization cannot be reversed. Infrared, UV–vis diffuse spectroscopy, and thermal properties were also measured. Crystal data: $BaMgTe_2O_7$, orthorhombic, space group *Ama*2 (No. 40), a = 5.558(2) Å, b = 15.215(6) Å, c = 7.307(3) Å, V = 617.9(4) Å^3, and Z = 4; $BaZnTe_2O_7$, orthorhombic, space group *Ama*2 (No. 40), a = 5.5498(4) Å, b = 15.3161(11) Å, c = 7.3098(5) Å, V = 621.34(8) Å^3, and Z = 4.

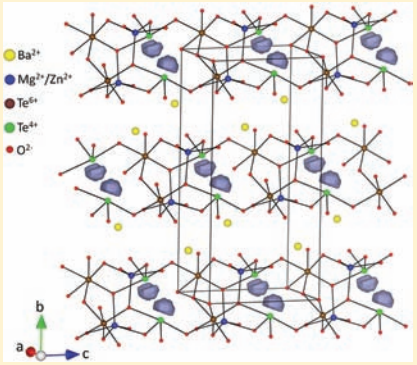

INTRODUCTION

Polar noncentrosymmetric (NCS) materials are of academic and commercial interest attributable to their technologically relevant functional properties. These include ferroelectricity, pyroelectricity, and non-linear optical behavior.[1−5] Crystallographically, a material may be considered polar if it is found in one of 10 polar crystal classes (1, 2, 3, 4, 5, m, mm2, 3 m, 4 mm, or 6 mm).[6] Specific polar directions with each of these crystal classes have been defined. With respect to functional properties, ferroelectricity and pyroelectricity may be observed and are exclusive to polar materials. Second-order non-linear optical behavior and piezoelectricity are also observed in polar materials; however, with these functionalities polarity is not required, but the material must be NCS.[5] For ferroelectric behavior, the observed macroscopic polarization may be reversed, or switched, in the presence of an external electric field,[1] whereas for pyroelectric behavior the magnitude of the macroscopic polarization changes as a function of temperature.[3] Thus, all ferroelectrics are pyroelectrics, but the converse is not true.

A number of design strategies have been discussed for creating new polar materials.[7−28] We have focused on synthesizing new oxide materials that contain cations susceptible to second-order Jahn–Teller (SOJT) distortions,[29−34] that is, octahedrally coordinated d^0 transition metals (Ti^{4+}, Nb^{5+}, W^{6+}, etc.) and cations with a stereoactive lone-pair (Se^{4+}, Te^{4+}, I^{5+}, etc.).[35−51] Attributable to SOJT effects, cations in both families are observed in asymmetric and polar coordination environments. When these coordination environments "constructively align" in the crystal structure, a macroscopically polar material is created.

Recently, we reported on the synthesis, characterization, and functional properties of $ACuTe_2O_7$ (A = Sr^{2+}, Ba^{2+}, and Pb^{2+}).[50] We determined that the specific A^{2+} cation plays a crucial role in the macroscopic polarity of the material. In fact, only $BaCuTe_2O_7$ is polar. In expanding this research toward the synthesis of new polar oxides, we attempted to replace Cu^{2+}, in $BaCuTe_2O_7$, with Mg^{2+} or Zn^{2+}. In this paper, we report on the synthesis, characterization, and functional properties of two new polar oxides: $BaMgTe_2O_7$ and $BaZnTe_2O_7$. Although both materials are polar, we demonstrate that the compounds are not ferroelectric. Additional functional properties, such as piezoelectric, pyroelectric, and powder SHG, were investigated.

EXPERIMENTAL SECTION

Reagents. $BaCO_3$ (Aldrich, 99+%), $MgCO_3$ (Fisher, 99+%), ZnO (Alfa Aesar, 99.99%), TeO_2 (GFS Chemicals, 99.5+%), and $H_2TeO_4 \cdot 2H_2O$ (Alfa Aesar, 99+%) were used as received.

Syntheses. Polycrystalline samples of $BaMgTe_2O_7$ and $BaZnTe_2O_7$ were prepared by conventional solid-state methods. A stoichiometric mixture of $BaCO_3$ (0.592 g, 3.00 mmol), $MgCO_3$

Received: December 2, 2011
Published: February 1, 2012

   dx.doi.org/10.1021/ic202602q | Inorg. Chem. 2012, 51, 2662–2668

(ZnO) (0.253 g, 3.00 mmol) (0.244 g, 3.00 mmol), TeO_2 (0.479 g, 3.00 mmol), and $H_2TeO_4 \cdot 2H_2O$ (0.675 g, 3.00 mmol) were thoroughly ground and pressed into pellets. The pellets were placed in alumina crucibles and heated to 650 °C in air, held for 3 d, and then cooled to room temperature. Purity was confirmed by powder X-ray diffraction.

Single crystals of $BaMgTe_2O_7$ and $BaZnTe_2O_7$ were grown from reaction mixtures using conventional solid-state methods. Mixtures of 0.529 g (0.569 g) (1.00 mmol (1.00 mmol)) of $BaMgTe_2O_7$ ($BaZnTe_2O_7$), and 0.319 g (0.160 g) (2.00 mmol (1.00 mmol)) of TeO_2 were placed in a platinum crucible. The crucible was gradually heated to 730 °C in air, held for 12 h, and then cooled slowly to 400 °C at a rate of 1.5 °C h^{-1} followed by rapid cooling to room temperature. For $BaMgTe_2O_7$ and $BaZnTe_2O_7$, plate-shaped colorless crystals were recovered in a yield of ~20% based on $BaMTe_2O_7$ (M = Mg^{2+} and Zn^{2+}). Impurities of $BaTe_2O_6$,[52] TeO_2,[53] and an unidentified phase were also found.

Single Crystal X-ray Diffraction. Crystals of $BaMgTe_2O_7$ (0.08 × 0.08 × 0.1 mm) and $BaZnTe_2O_7$ (0.06 × 0.06 × 0.08 mm) were used for single crystal data collection. Data were collected using a Siemens SMART diffractometer equipped with a 1K CCD area detector using graphite−monochromated Mo Kα radiation. A hemisphere of data was collected using a narrow−frame method with scan widths of 0.30° in ω and an exposure time of 30 s per frame for both $BaMgTe_2O_7$ and $BaZnTe_2O_7$. The data were integrated using the Siemens SAINT program,[54] with the intensities corrected for Lorentz, polarization, air absorption, and absorption attributable to the variation in the path length through the detector faceplate. ψ−scans for the reported materials were used for the absorption correction on the hemisphere of data. All of the data were solved by direct methods using SHELXS-97 and refined using SHELXL-97.[55,56] All of the atoms were refined with anisotropic thermal parameters and converged for $I > 2\sigma$. All calculations were performed using the WinGX-98 crystallographic software package.[57] Crystallographic data are given in Tables 1 and 2.

Table 1. Crystallographic Data for $BaMgTe_2O_7$ and $BaZnTe_2O_7$

	$BaMgTe_2O_7$	$BaZnTe_2O_7$
fw	528.85	569.91
crystal system	orthorhombic	orthorhombic
space group	*Ama*2 (No. 40)	*Ama*2 (No. 40)
a (Å)	5.558(2)	5.5498(4)
b (Å)	15.215(6)	15.3161(11)
c (Å)	7.307(3)	7.3098(5)
α (deg)	90	90
β (deg)	90	90
γ (deg)	90	90
V (Å^3)	617.9(4)	621.34(8)
Z	4	4
R (int)	0.0334	0.0441
GOF (F^2)	1.195	1.161
Flack parameter	−0.002(10)	−0.003(4)
$R(F)^a$	0.0183	0.0163
$R_w(F_o^2)^b$	0.0483	0.0457

$^aR(F) = \sum||F_o| - |F_c||/\sum|F_o|$. $^bR_w(F_o^2) = [\sum w(F_o^2 - F_c^2)^2/\sum w(F_o^2)^2]^{1/2}$.

Powder X-ray Diffraction. Powder X-ray diffraction (PXRD) data of the materials were collected using a PANalytical X'Pert PRO diffractometer operating with Cu Kα radiation. The data were taken in the 2θ range of 5−70° in a continuous scanning mode. No impurities were observed, and the calculated and experimental PXRD patterns are in excellent agreement (See Supporting Information, Figure S1).

Infrared Spectroscopy. IR spectra were recorded on a Matterson FTIR 5000 spectrometer in the 400−4000 cm^{-1} range.

Table 2. Selected Bond Distances (Å) for $BaMgTe_2O_7$ and $BaZnTe_2O_7$

$BaMgTe_2O_7$		$BaZnTe_2O_7$	
Ba(1)−O(1) × 2	2.990(2)	Ba(1)−O(1) × 2	3.001(2)
Ba(1)−O(2) × 2	2.821(6)	Ba(1)−O(2) × 2	2.823(4)
Ba(1)−O(2) × 2	3.004(7)	Ba(1)−O(2) × 2	2.999(5)
Ba(1)−O(4) × 2	2.785(7)	Ba(1)−O(4) × 2	2.788(5)
Ba(1)−O(4) × 2	2.847(6)	Ba(1)−O(4) × 2	2.834(5)
Te(1)−O(1)	1.977(9)	Te(1)−O(1)	1.969(8)
Te(1)−O(3)	1.903(5)	Te(1)−O(3)	1.907(5)
Te(1)−O(4) × 2	1.874(7)	Te(1)−O(4) × 2	1.870(5)
Te(1)−O(5) × 2	2.007(2)	Te(1)−O(5) × 2	2.000(2)
Te(2)−O(1)	1.987(10)	Te(2)−O(1)	1.999(8)
Te(2)−O(2) × 2	1.837(8)	Te(2)−O(2) × 2	1.846(5)
Te(2)−O(3)	2.335(4)	Te(2)−O(3)	2.295(5)
Mg(1)−O(2) × 2	2.049(8)	Zn(1)−O(2) × 2	2.079(5)
Mg(1)−O(3)	2.028(6)	Zn(1)−O(3)	2.031(5)
Mg(1)−O(4) × 2	2.001(8)	Zn(1)−O(4) × 2	2.015(5)

UV−vis Diffuse Reflectance Spectroscopy. UV−vis reflectance data were collected on a Varian Cary 500 Scan UV−vis−NIR spectrophotometer over the spectral range 200−2000 nm at room temperature. Poly(tetrafluoroethylene) was used as a reference material. Reflectance spectra were converted to absorbance using the Kubelka−Munk function.[58]

Thermal Analyses. Thermogravimetric analysis (TGA) and differential thermal analysis (DTA) were carried out on EXSTAR TG/DTA 6300 series (SII Nano Technology Inc.). Approximately 20 mg of the samples were placed into a platinum crucible and heated and cooled between room temperature and 900 °C at a rate of 10 °C min^{-1} under flowing nitrogen gas.

Second-Harmonic Generation (SHG). Powder SHG measurements were performed on a modified Kurtz-NLO system using a pulsed Nd:YAG laser with a wavelength of 1064 nm. A detailed description of the equipment and methodology has been published elsewhere.[5] As powder SHG efficiency has been shown to depend strongly on particle size, the reported materials were ground and sieved into distinct particle size ranges (<20, 20−45, 45−63, 63−75, 75−90, >90 μm). Comparisons with known SHG materials were made by grinding and sieving crystalline α-SiO_2 and $LiNbO_3$ into the same particle size ranges. No index matching fluid was used in any of the experiments.

Piezoelectric Measurements. Converse piezoelectric measurements were performed using a Radiant Technologies RT66A piezoelectric test system with a TREK high voltage amplifier, Precision Materials Analyzer, Precision High Voltage Interface, and MTI 2000 Fotonic Sensor. The reported materials were pressed into pellets (~1.3 cm diameter, ~1 mm thick) and sintered at 650 °C for 2 days, respectively. Silver paste was applied to both sides of the pellets, and the pellets were cured at 300 °C for 12 h. The same pellets were also used in polarization measurements.

Polarization Measurements. The polarization was measured on a Radiant Technologies RT66A ferroelectric test system with a TREK high voltage amplifier between room temperature and 215 °C in a Delta 9023 environmental test chamber. The unclamped pyroelectric coefficient, defined as dP/dT (change in polarization with respect to the change in temperature), was determined by measuring the polarization as a function of temperature. A detailed description of the methodology used has been published elsewhere.[5] To measure any possible ferroelectric behavior, the polarization was measured at room temperature under a static electric field of 9−12 kV/cm between 20−200 Hz. For the pyroelectric measurements, the polarization was measured statically from room temperature to 215 °C in 10 °C

dx.doi.org/10.1021/ic202602q | Inorg. Chem. 2012, 51, 2662−2668

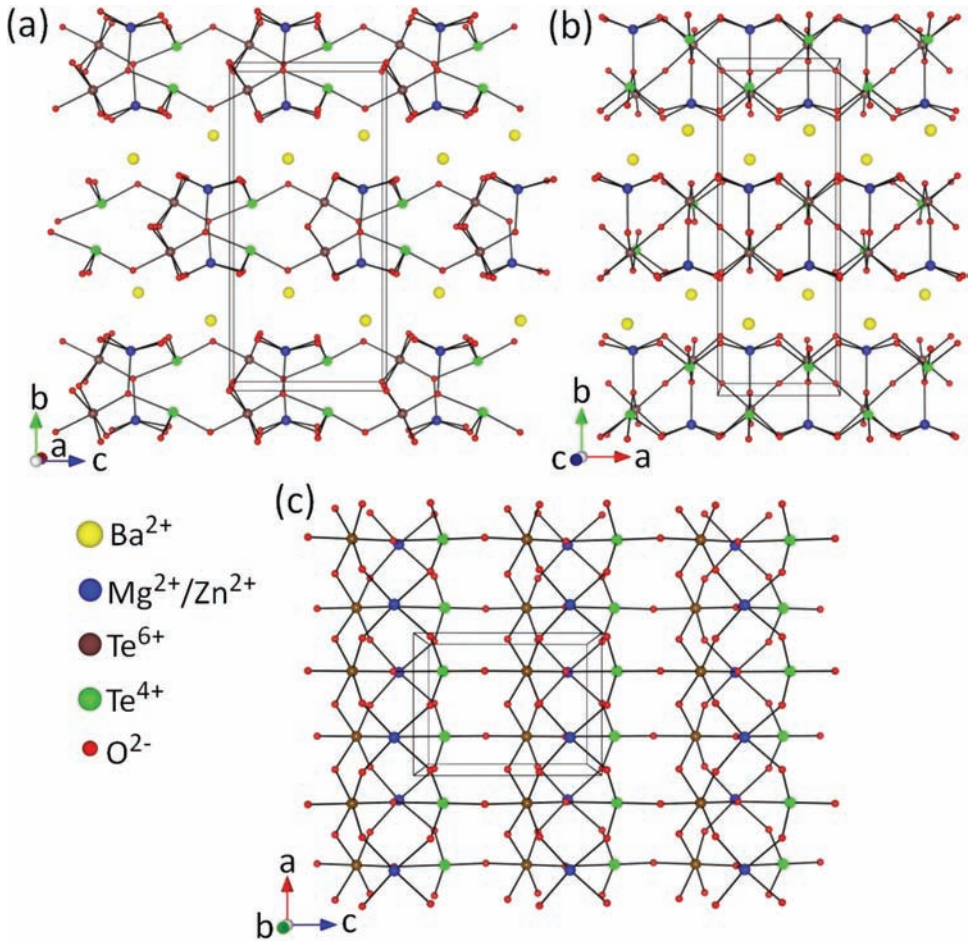

Figure 1. Ball-and-stick diagram of $BaMTe_2O_7$ (M = Mg^{2+} or Zn^{2+}) in the (a) *bc*- and (b) *ab*-plane. The two-dimensional layer in the *ac*-plane is shown in (c).

increments, with an electric field of 7−9 kV/cm. The temperature was allowed to stabilize before the polarization was measured.

For all of the structural figures and electronic structure results, the program VESTA was utilized.[59]

RESULTS AND DISCUSSION

Structures. $BaMTe_2O_7$ (M = Mg^{2+} and Zn^{2+}) are isostructural with the previously reported $BaCuTe_2O_7$,[50,60] and exhibit a crystal structure composed of layers of corner-shared MO_5 (M = Mg^{2+} or Zn^{2+}) square pyramids, TeO_6 octahedra, and TeO_4 polyhedra. The $[MTe_2O_7]^{2-}$ anionic layers (M = Mg^{2+} and Zn^{2+}) stack along the *b*-axis, and are separated by Ba^{2+} cations (see Figures 1a and 1b). One-dimensional zigzag chains of corner-shared $Te(1)O_6$ polyhedra are observed along the *a*-axis, and are corner-shared to $Te(2)O_4$ polyhedra along the *c*-axis. This array results in a two-dimensional layer in the *ac*-plane where MO_5 (M = Mg^{2+} or Zn^{2+}) polyhedra alternate above and below the layer (see Figure 1c). In connectivity terms, the materials can be described as $[(MO_{4/2}O_{1/3})^{2.666-}(Te(1)O_{5/2}O_{1/3})^{0.333}\ (Te(2)O_{3/2}O_{1/3})^{0.333}]^{2-}$ (M = Mg^{2+} and Zn^{2+}), with the charge balance maintained by one Ba^{2+} cation. The M^{2+} (M = Mg and Zn) cations are found in a square pyramidal coordination environment with M−O bond distances ranging from 2.001(8) Å to 2.079(5) Å. The $Te(1)^{6+}$ cation is observed in octahedral coordination with Te(1)−O bond distances of 1.870(5)−2.007(2) Å, whereas the $Te(2)^{4+}$ cation is found in a highly asymmetric coordination environment, attributable to its stereoactive lone-pair, and is bonded to four oxygen atoms with Te(2)−O bond distances ranging between 1.837(8)−2.335(4) Å. To examine the lone-pair character on the Te^{4+} cation, electron localization function (ELF)[61,62] calculations were performed. Figure 2 clearly shows the iso-surfaces for η = 0.9 around the Te^{4+} cation that may be considered as a stereoactive lone-pair. The Ba^{2+} cation is surrounded by 10 oxygen atoms with Ba−O distances between 2.785(7) Å and 3.004(7) Å. Bond valence calculations[63,64] resulted in values of 2.00−2.04, 5.69−5.78, 4.14−4.23, and 2.01−2.03 for M^{2+} (M = Mg and Zn), $Te(1)^{6+}$, $Te(2)^{4+}$, and Ba^{2+}, respectively, in both materials. Detailed bond valence calculation results are given in Supporting Information, Table S2.

Dipole Moments and BSI/GII Values. To understand the origin of the macroscopic polarity, we examined the local dipole moments[65,66] in the individual coordination polyhedra, as well as the alignment of these polyhedra. As summarized in Table 3, the values of each cation are naturally similar attributable to the iso-structural nature of the materials. Although several types of metal oxide polyhedra are present, MO_5 (M = Mg^{2+} and Zn^{2+}) square pyramids, TeO_6 octahedra, and TeO_4 seesaw polyhedra, it is the latter, the TeO_4 polyhedra, that is the main contributor the macroscopic polarity. The MO_5 square pyramids, although locally polar, are oriented in nearly opposite directions (see Figure 3), thus canceling any net polarization, whereas the TeO_6 octahedron is nearly ideal and generates minimal

dx.doi.org/10.1021/ic202602q | Inorg. Chem. 2012, 51, 2662−2668

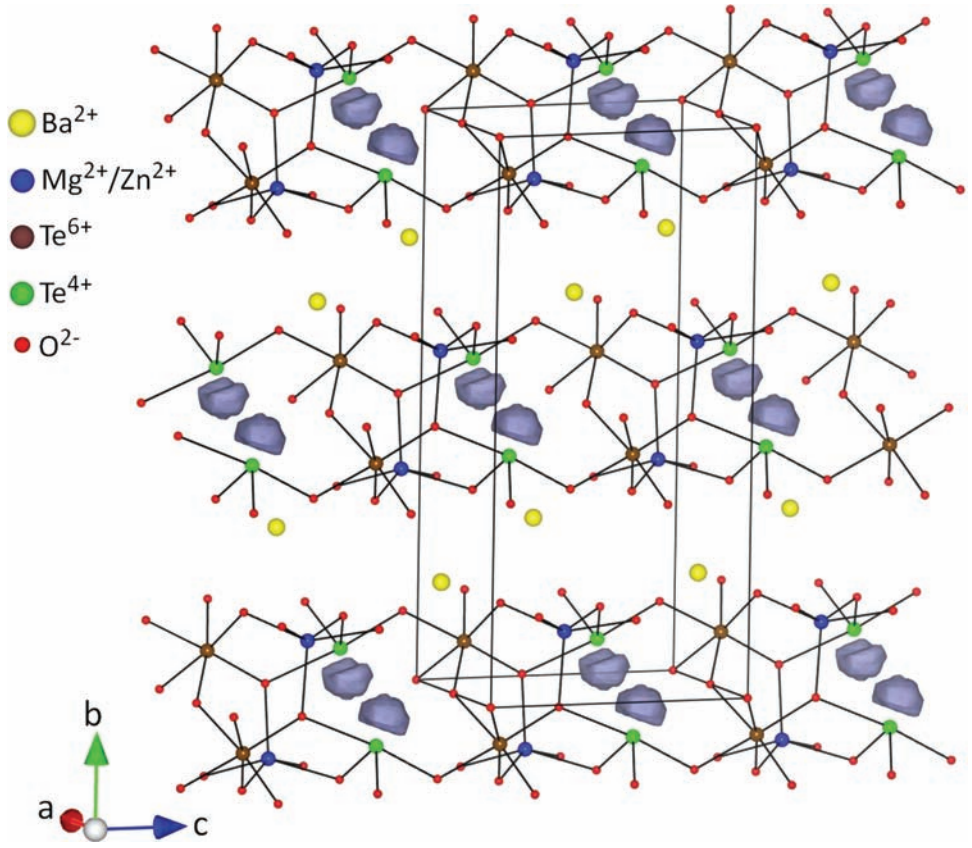

Figure 2. Electron localization function (ELF) isosurfaces with η = 0.9 is shown. The lobe-like iso-surface indicates that the lone-pair on the Te^{4+} cations is stereoactive.

Table 3. BVS, BSI, and GII Values, Dipole Moments, SHG Efficiencies (Relative to α-SiO_2), Piezoelectric Constants (pm/V), and Pyroelectric Coefficients ($\mu C/m^2 \cdot K$ at 65 °C) for $BaMTe_2O_7$ (M = Mg^{2+} and Zn^{2+})

	BVS						dipole moments					
compounds	Ba^{2+}	M^{2+}	$Te(1)^{6+}$	$Te(2)^{4+}$	BSI	GII	M^{2+}	$Te(1)^{6+}$	$Te(2)^{4+}$	SHG	piezo. d_{33}	pyro. coeff.
$BaMgTe_2O_7$	2.03	2.04	5.70	4.16	0.095	0.193	1.36	3.44	10.1	230	70	−18
$BaZnTe_2O_7$	2.01	2.00	5.76	4.22	0.096	0.171	1.53	3.46	10.1	200	57	−10

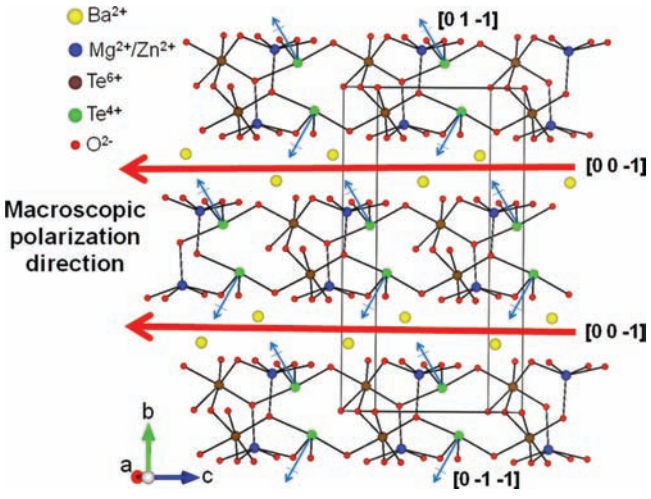

Figure 3. Ball-and-stick representation of $BaMTe_2O_7$ (M = Mg^{2+} or Zn^{2+}). Note that the TeO_4 polyhedra exhibit local dipole moment (blue arrows) in the [0 1 −1] and [0 −1 −1] directions. As a result macroscopic polarization is exhibited along the [0 0 −1] direction.

polarization. The dipole moments associated with the TeO_4 polyhedra are directed along the approximate [0−1−1] and [01−1] directions, resulting in a net polarization moment toward the [00−1]. This direction is consistent with the defined polar direction in crystal class mm2.[6] The fact that the TeO_4 polyhedra are mainly responsible for the macroscopic polarization profoundly impacts the associated functional properties, as will be discussed later.

In addition to the dipole moment calculations, the bond strain and global instability indices, BSI[67] and GII,[68] respectively, were calculated. The BSI and GII are indicators of electronic- and lattice-induced strains, respectively. A material is considered strained if BSI and GII values are greater than 0.05 valence units (vu). For both materials, the GII values are substantially larger than the BSI values. This indicates that the lattice-induced strains are stronger than the electronic-induced strains. It is expected that the GII > BSI, as the materials have only one cation that can undergo a SOJT distortion, Te^{4+}.

Infrared Spectroscopy. The IR spectra of $BaMgTe_2O_7$ and $BaZnTe_2O_7$ indicate Te−O and M−O (M = Mg^{2+} and Zn^{2+}) vibrations between 400−900 cm^{-1}. The bands above 600 cm^{-1} can be assigned to Te^{4+}−O and Te^{6+}−O stretching,

dx.doi.org/10.1021/ic202602q | Inorg. Chem. 2012, 51, 2662−2668

whereas the bands below 600 cm^{-1} can be attributed to Te^{6+}–O anti–stretching and Te^{6+}–O–Te^{6+} or M^{2+}–O vibrations. These assignments are consistent with those reported previously.[38,39,69] The IR spectra and assignments are shown in Supporting Information, Figure S2.

UV–vis Diffuse Reflectance Spectroscopy. As $BaMgTe_2O_7$ and $BaZnTe_2O_7$ are white, it is expected that the absorption energy for the materials is over 3 eV. Absorption (K/S) data were calculated from the Kubelka–Munk function:[58]

$$F(R) = \frac{(1-R)^2}{2R} = \frac{K}{S}$$

with R representing the reflectance, K the absorption, and S the scattering. In a K/S versus E (eV) plot, extrapolating the linear part of the rising curve to zero provides the onset of absorption at 3.39 and 3.37 eV for $BaMgTe_2O_7$ and $BaZnTe_2O_7$, respectively, indicating the insulating nature of the materials. The UV–vis diffuse reflectance spectra for the reported materials are shown in Supporting Information, Figure S3.

Thermal Analyses. Thermogravimetric analysis (TGA) and differential thermal analysis (DTA) were investigated to characterize thermal behavior of $BaMTe_2O_7$ (M = Mg^{2+} and Zn^{2+}). Both materials are stable up to 700 °C, and the DTA data indicate the materials melt incongruently. The thermal decomposition products were $Ba_2Te_3O_8$,[70] $BaTeO_3$,[71] and Mg_3TeO_6[72] for $BaMgTe_2O_7$, and $Ba_2Te_3O_8$,[70] $BaTeO_3$,[71] $BaTe_4O_9$,[73] and $BaTe_2O_5$[74] for $BaZnTe_2O_7$, respectively, as confirmed by powder X-ray diffraction. The TGA and DTA data have been given in Supporting Information, Figure S4.

Second-Harmonic Generation (SHG) and Piezoelectricity. SHG and piezoelectric measurements were performed on the reported materials. Powder SHG measurements using 1064 nm radiation revealed SHG efficiencies of approximately 6 and 5 × KDP, or 230 and 200 × α-SiO_2, for $BaMgTe_2O_7$ and $BaZnTe_2O_7$, respectively, in the particle size range of 45–63 μm. The moderate SHG efficiencies may be attributed to the alignment of the asymmetric and polar TeO_4 polyhedra. Additional SHG measurements with particle sizes between 20–125 μm reveal that the materials exhibit type I phase-matching behavior, and fall into the class C category of SHG materials (see Supporting Information, Figure S5).[75] On the basis of SHG efficiencies and phase-matching behaviors, the average NLO susceptibility, $\langle d_{eff}\rangle_{exp}$, of approximately 18 and 16 pm/V for $BaMgTe_2O_7$ and $BaZnTe_2O_7$, respectively, were estimated. Also, converse piezoelectric measurements revealed d_{33} piezoelectric charge constants of 70 and 57 pm/V for $BaMgTe_2O_7$ and $BaZnTe_2O_7$, respectively (see Supporting Information, Figure S6).

Polarization Measurements. Polarization measurements were performed to examine any ferroelectric and pyroelectric phenomena. Frequency dependent polarization measurements indicated that the materials are *not* ferroelectric, that is, the observed macroscopic polarization cannot be reversed under an external electric field. The observed loops are not attributable to ferroelectric hysteresis, but are rather likely owing to dielectric loss (see Supporting Information, Figure S7).[76] To better understand this lack of polarization reversal, it is highly relevant to examine the local coordination environment of the TeO_4 polyhedra. Recall that the macroscopic polarity in both materials is attributable to the "constructive addition" of the dipole moments associated with the polar TeO_4 polyhedra. Macroscopic polarization reversal would imply microscopic polarization reversal of the TeO_4 polyhedra. For ferroelectric behavior to occur, inversion of the individual TeO_4 polyhedra is necessary (see Figure 4a). Assuming no Te–O bonds are broken, one possible manner for this to occur is through an umbrella-type inversion of the polyhedra. We previously demonstrated that for SeO_3 polyhedra an umbrella-type inversion is energetically unfavorable attributable to the high energy barrier compared with known ferroelectrics such as $BaTiO_3$ and $PbTiO_3$.[77] If we use the same ideas, qualitatively, with an umbrella-type mechanism for the TeO_4 polyhedra, we note that the O2 atoms need to move to the opposite side of the Te^{4+} cation for polarization inversion. This movement, however, requires simultaneous movement of large structural units (see Figure 4b) resulting in a substantial rearrangement of atoms and bonds. It is suggested that this movement would require a large amount of energy, similar to the inversion of a SeO_3 polyhedron. As such, the macroscopic polarization observed in both $BaMgTe_2O_7$ and $BaZnTe_2O_7$ is not reversible. Although the materials are not ferroelectric, they are polar and thus exhibit a macroscopic polarization. Thus, pyroelectric measurements were performed to investigate the magnitude of the polarization as a function of temperature. Pyroelectric coefficients (p), defined as a change in polarization as a function of temperature, was measured. Values of −18 and −10 $\mu C \cdot m^{-2} \cdot K^{-1}$ were determined for $BaMgTe_2O_7$ and $BaZnTe_2O_7$ respectively. These values are in agreement with other nonferroelectric pyroelectric materials, for example, ZnO (−9.4 $\mu C \cdot m^{-2} \cdot K^{-1}$) and tourmaline (−4.0 $\mu C \cdot m^{-2} \cdot K^{-1}$) (see Supporting Information, Figures S8 and S9).[3]

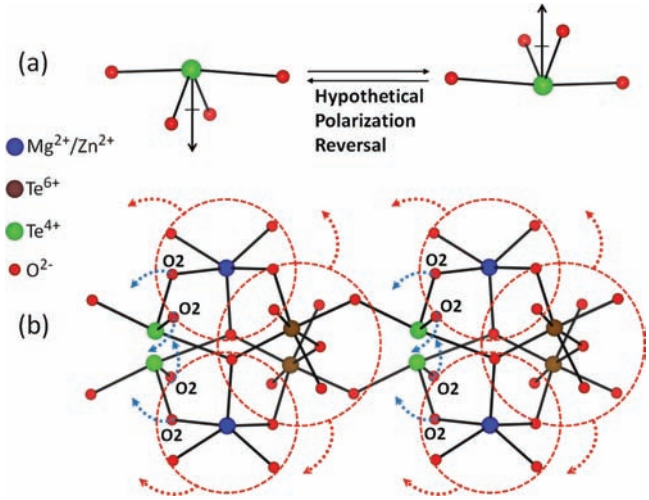

Figure 4. Ball-and-stick figures of hypothetical polarization reversal. Note that if the TeO_4 polarization reversal occurs, (a) and blue dotted arrows in (b), large movements of MO_5 (M = Mg^{2+} or Zn^{2+}) and TeO_6 polyhedra, red dotted arrows and circles in (b), are expected.

CONCLUSIONS

We have successfully synthesized and characterized two new NCS polar oxide materials, $BaMgTe_2O_7$ and $BaZnTe_2O_7$. The iso-structural materials exhibit a two-dimensional topology that contains MO_5 (M = Mg^{2+} or Zn^{2+}), TeO_6, and TeO_4 polyhedra. The observed macroscopic polarity is attributable to the alignment of the polar TeO_4 polyhedra. Attributable to this alignment, a moderate SHG efficiency of approximately 5 ×

dx.doi.org/10.1021/ic202602q | Inorg. Chem. 2012, 51, 2662–2668

KDP, or 200 × α-SiO_2, is observed. Although both materials are polar, the materials are *not* ferroelectric, that is, the macroscopic polarization is not reversible.

■ ASSOCIATED CONTENT

Supporting Information

X-ray data in CIF format, powder XRD patterns, IR and UV−vis spectra, TGA and DTA diagrams, piezoelectric and polarization loops, and detailed bond valence result tables. This material is available free of charge via the Internet at http://pubs.acs.org.

■ AUTHOR INFORMATION

Corresponding Author

*E-mail: psh@uh.edu.

■ ACKNOWLEDGMENTS

We thank the Robert A. Welch Foundation (Grant E-1457) and the Texas Center for Superconductivity for support. J.Y. thanks International Centre for Diffraction Data for a 2011 Ludo Frevel Crystallography Scholarship Award.

■ REFERENCES

(1) Auciello, O.; Scott, J. F.; Ramesh, R. *Phys. Today* **1998**, *51*, 22.
(2) Haertling, G. H. *J. Am. Ceram. Soc.* **1999**, *82*, 797.
(3) Lang, S. B.; Das-Gupta, D. K. In *Handbook of Advanced Electronic and Photonic Materials and Devices*; Nalwa, H. S., Ed.; Academic Press: San Francisco, CA, 2001; Vol. *4*.
(4) Lang, S. B. *Phys. Today* **2005**, *58*, 31.
(5) Ok, K. M.; Chi, E. O.; Halasyamani, P. S. *Chem. Soc. Rev.* **2006**, *35*, 710.
(6) Hahn, T. *International Tables for Crystallography*; Kluwer Academic: Dordrecht, The Netherlands, 2006; Vol. *A*, Space Group Symmetry.
(7) Welk, M. E.; Norquist, A. J.; Stern, C. L.; Poeppelmeier, K. R. *Inorg. Chem.* **2001**, *40*, 5479.
(8) Welk, M. E.; Norquist, A. J.; Arnold, F. P.; Stern, C. L.; Poeppelmeier, K. R. *Inorg. Chem.* **2002**, *41*, 5119.
(9) Izumi, H. K.; Kirsch, J. E.; Stern, C. L.; Poeppelmeier, K. R. *Inorg. Chem.* **2005**, *44*, 884.
(10) Muller, E. A.; Cannon, R. J.; Sarjeant, A. N.; Ok, K. M.; Halasyamani, P. S.; Norquist, A. J. *Cryst. Growth Des.* **2005**, *5*, 1913.
(11) Kong, F.; Huang, S.-P.; Sun, Z.-M.; Mao, J.-G.; Cheng, W.-D. *J. Am. Chem. Soc.* **2006**, *128*, 7750.
(12) Veltman, T. R.; Stover, A. K.; Sarjeant, A. N.; Ok, K. M.; Halasyamani, P. S.; Norquist, A. J. *Inorg. Chem.* **2006**, *45*, 5529.
(13) Cooper, V. R.; Johnston, K.; Rabe, K. M. *Phys. Rev. B: Condens. Matter Mater. Phys.* **2007**, *76*, 020103/1.
(14) Marvel, M. R.; Lesage, J.; Baek, J.; Halasyamani, P. S.; Stern, C. L.; Poeppelmeier, K. R. *J. Am. Chem. Soc.* **2007**, *129*, 13963.
(15) Inaguma, Y.; Yoshida, M.; Katsumata, T. *J. Am. Chem. Soc.* **2008**, *130*, 6704.
(16) Choyke, S. J.; Blau, S. M.; Larner, A. A.; Narducci, S. A.; Yeon, J.; Halasyamani, P. S.; Norquist, A. J. *Inorg. Chem.* **2009**, *48*, 11277.
(17) Claridge, J. B.; Hughes, H.; Bridges, C. A.; Allix, M.; Suchomel, M. R.; Niu, H.; Kuang, X.; Rosseinsky, M. J.; Bellido, N.; Grebille, D.; Perez, O.; Simon, C.; Pelloquin, D.; Blundell, S. J.; Lancaster, T.; Baker, P. J.; Pratt, F. L.; Halasyamani, P. S. *J. Am. Chem. Soc.* **2009**, *131*, 14000.
(18) Eklund, C. J.; Fennie, C. J.; Rabe, K. M. *Phys. Rev. B: Condens. Matter Mater. Phys* **2009**, *79*, 220101/1.
(19) Sun, C.-F.; Hu, C.-L.; Xu, X.; Ling, J.-B.; Hu, T.; Kong, F.; Long, X.-F.; Mao, J.-G. *J. Am. Chem. Soc.* **2009**, *131*, 9486.
(20) Bera, T. K.; Jang, J. I.; Song, J.-H.; Malliakas, C. D.; Freeman, A. J.; Ketterson, J. B.; Kanatzidis, M. G. *J. Am. Chem. Soc.* **2010**, *132*, 3484.
(21) Chung, I.; Jang, J.-I.; Malliakas, C. D.; Ketterson, J. B.; Kanatzidis, M. G. *J. Am. Chem. Soc.* **2010**, *132*, 384.
(22) Huang, Y.-Z.; Wu, L.-M.; Wu, X.-T.; Li, L.-H.; Chen, L.; Zhang, Y.-F. *J. Am. Chem. Soc.* **2010**, *132*, 12788.
(23) Li, P.-X.; Kong, F.; Hu, C.-L.; Zhao, N.; Mao, J.-G. *Inorg. Chem.* **2010**, *49*, 5943.
(24) Yang, T.; Sun, J.; Yeon, J.; Halasyamani, P. S.; Huang, S.; Hemberger, J.; Greenblatt, M. *Chem. Mater.* **2010**, *22*, 4814.
(25) Benedek, N. A.; Fennie, C. J. *Phys. Rev. Lett.* **2011**, *106*, 107204/1.
(26) Leblanc, N.; Mercier, N.; Zorina, L.; Simonov, S.; Auban-Senzier, P.; Pasquier, C. *J. Am. Chem.. Soc.* **2011**, *133*, 14924.
(27) Sun, C.-F.; Hu, C.-L.; Xu, X.; Yang, B.-P.; Mao, J.-G. *J. Am. Chem. Soc.* **2011**, *133*, 5561.
(28) Wu, H.; Pan, S.; Poeppelmeier, K. R.; Li, H.; Jia, D.; Chen, Z.; Fan, X.; Yang, Y.; Rondinelli, J. M.; Luo, H. *J. Am. Chem. Soc.* **2011**, *133*, 7786.
(29) Opik, U.; Pryce, M. H. L. *Proc. R. Soc. A* **1957**, *238*, 425.
(30) Bader, R. F. W. *Mol. Phys.* **1960**, *3*, 137.
(31) Bader, R. F. W. *Can. J. Chem.* **1962**, *40*, 2140.
(32) Pearson, R. G. *J. Am. Chem. Soc.* **1969**, *91*, 4947.
(33) Pearson, R. G. *THEOCHEM* **1983**, *12*, 25.
(34) Wheeler, R. A.; Whangbo, M. H.; Hughbanks, T.; Hoffmann, R.; Burdett, J. K.; Albright, T. A. *J. Am. Chem. Soc.* **1986**, *108*, 2222.
(35) Porter, Y.; Halasyamani, P. S. *J. Solid State Chem.* **2003**, *174*, 441.
(36) Ra, H.-S.; Ok, K. M.; Halasyamani, P. S. *J. Am. Chem. Soc.* **2003**, *125*, 7764.
(37) Ok, K. M.; Halasyamani, P. S. *Angew. Chem., Int. Ed.* **2004**, *43*, 5489.
(38) Chi, E. O.; Ok, K. M.; Porter, Y.; Halasyamani, P. S. *Chem. Mater.* **2006**, *18*, 2070.
(39) Kim, J.-H.; Baek, J.; Halasyamani, P. S. *Chem. Mater.* **2007**, *19*, 5637.
(40) Sivakumar, T.; Chang, H. Y.; Baek, J.; Halasyamani, P. S. *Chem. Mater.* **2007**, *19*, 4710.
(41) Chang, H. Y.; Sivakumar, T.; Ok, K. M.; Halasyamani, P. S. *Inorg. Chem.* **2008**, *47*, 8511.
(42) Chang, H. Y.; Kim, S.-H.; Ok, K. M.; Halasyamani, P. S. *Chem. Mater.* **2009**, *21*, 1654.
(43) Chang, H.-Y.; Kim, S.-H.; Halasyamani, P. S.; Ok, K. M. *J. Am. Chem. Soc.* **2009**, *131*, 2426.
(44) Chang, H.-Y.; Kim, S.-H.; Ok, K. M.; Halasyamani, P. S. *J. Am. Chem. Soc.* **2009**, *131*, 6865.
(45) Kim, S.-H.; Yeon, J.; Halasyamani, P. S. *Chem. Mater.* **2009**, *21*, 5335.
(46) Chang, H. Y.; Kim, S. W.; Halasyamani, P. S. *Chem. Mater.* **2010**, *22*, 3241.
(47) Yeon, J.; Kim, S.-H.; Halasyamani, P. S. *Inorg. Chem.* **2010**, *49*, 6986.
(48) Nguyen, S. D.; Kim, S.-H.; Halasyamani, P. S. *Inorg. Chem.* **2011**, *50*, 5215.
(49) Nguyen, S. D.; Yeon, J.; Kim, S.-H.; Halasyamani, P. S. *J. Am. Chem. Soc.* **2011**, *133*, 12422.
(50) Yeon, J.; Kim, S.-H.; Hayward, M. A.; Halasyamani, P. S. *Inorg. Chem.* **2011**, *50*, 8663.
(51) Zhang, W.; Halasyamani, P. S.; Gao, Z.; Wang, S.; Wang, J.; Tao, X. *Cryst. Growth Des.* **2011**, *11*, 3636.
(52) Kocak, M.; Platte, C.; Troemel, M. *Acta Crystallogr., Sect. B* **1979**, *B35*, 1439.
(53) Lindqvist, O. *Acta Chem. Scand.* **1968**, *22*, 977.
(54) *SAINT, Program for Area Detector Absorption Correction*, version 4.05; Siemens Analytical X-ray Systems: Madison, WI, 1995.
(55) Sheldrick, G. M. *SHELXL-97, A Program for Crystal Structure Refinement*; University of Göttingen: Göttingen, Germany, 1997.
(56) Sheldrick, G. M. *SHELXS-97, A Program for Automatic Solution of Crystal Structures*; University of Göttingen: Göttingen, Germany, 1997.
(57) Farrugia, L. J. *J. Appl. Crystallogr.* **1999**, *32*, 837.

(58) Kubelka, P.; Munk, F. Z. *Tech. Phys.* **1931**, *12*, 593.
(59) Momma, K.; Izumi, F. *J. Appl. Crystallogr.* **2008**, *41*, 653.
(60) Sedello, O.; Mueller-Buschbaum, H. *Z. Naturforsch., B: Chem. Sci.* **1996**, *51*, 465.
(61) Becke, A. D.; Edgecombe, K. E. *J. Chem. Phys.* **1990**, *92*, 5397.
(62) Silvi, B.; Savin, A. *Nature* **1994**, *371*, 683.
(63) Brown, I. D.; Altermatt, D. *Acta Crystallogr., Sect. B* **1985**, *B41*, 244.
(64) Brown, I. D. *The Chemical Bond in Inorganic Chemistry*; Oxford University Press: New York, 2002; Vol. *12*.
(65) Debye, P. *Phys. Z.* **1921**, *22*, 302.
(66) Debye, P. *Polar Molecules*; Chemical Catalog Company: New York, NY, 1929.
(67) Preiser, C.; Losel, J.; Brown, I. D.; Kunz, M.; Skowron, A. *Acta Crystallogr., Sect. B: Struct. Sci.* **1999**, *B55*, 698.
(68) Salinas-Sanchez, A.; Garcia-Munoz, J. L.; Rodriguez-Carvajal, J.; Saez-Puche, R.; Martinez, J. L. *J. Solid State Chem.* **1992**, *100*, 201.
(69) Porter, Y.; Halasyamani, P. S. *Inorg. Chem.* **2003**, *42*, 205.
(70) Agarwal, R.; Singh, Z. *J. Alloys Compd.* **2006**, *414*, 230.
(71) Folger, F. *Z. Anorg. Allg. Chem.* **1975**, *411*, 111.
(72) Schulz, H.; Bayer, G. *Acta Crystallogr., Sect. B* **1971**, *27*, 815.
(73) Johnston, M. G.; Harrison, W. T. A. *J. Am. Chem. Soc.* **2002**, *124*, 4576.
(74) Pashinkin, A. S. *Izv. Akad. Nauk SSSR, Neorg. Mater.* **1975**, *11*, 1650.
(75) Kurtz, S. K.; Perry, T. T. *J. Appl. Phys.* **1968**, *39*, 3798.
(76) Scott, J. F. *J. Phys.: Condens. Matter* **2008**, *20*, 021001/1.
(77) Cohen, R. E. *Nature* **1992**, *358*, 136.